Binding Effect of Surface-Modified Cadmium Sulfide on the Microstructure of PS-*b*-PEO Block Copolymers

U-Ser Jeng,* Ya-Sen Sun, Hsin-Yi Lee, Chia-Hung Hsu, and Keng S. Liang

National Synchrotron Radiation Research Center, 101 Hsin-Ann Road, Hsinchu Science Park, Hsinchu 30077, Taiwan

Siao-Wei Yeh and Kung-Hwa Wei

Department of Materials Science and Engineering, National Chiao Tung University, 1001 Ta Hsueh Road, Hsinchu 30050, Taiwan

Received February 10, 2004; Revised Manuscript Received April 7, 2004

ABSTRACT: CdS nanoparticles with surfaces modified by mercaptoethanol have been synthesized for greater solubility in dimethylformamide (DMF) and the ability to preferentially bind to the poly(ethylene oxide) (PEO) blocks of polystyrene-*block*-poly(ethylene oxide) (PS-*b*-PEO) copolymer. The size of the surface-modified CdS nanoparticles (M-CdS) in DMF can be characterized by the Schultz distribution of a mean radius of 18.4 Å and a polydispersity of 0.5, using small-angle X-ray scattering (SAXS). These M-CdS nanoparticles can further disperse in the PS-*b*-PEO, with a slightly larger mean radius than that observed in DMF. The uptake of M-CdS nanoparticles for the PEO blocks of the PS-*b*-PEO saturates around 7% in volume fraction. The binding of the nanoparticles promotes a segregation of the PEO/nanoparticles and leads to spherical PEO/M-CdS microdomains in the composite film with a greatly enhanced thermal stability. The structural information obtained from X-ray scattering agrees well with the transmission electron microscopy images and differential scanning calorimetry results.

1. Introduction

Semiconductor nanoparticles, with fascinating optical and electronic properties which originate from quantum confinement effects, attract much attention due to their possible application in, for example, photonic crystals[1] and light-emitting devices.[2,3] In these or other similar applications, the control of particle size, shape, and distribution/aggregation in practical devices becomes critical, since the quantum-confined optical and electronic properties may degrade due to the aggregation of nanoparticles. For dispersing nanoparticles, block copolymers, being able to self-assemble into various nanostructures through microphase separation, can serve as nanotemplates, provided that these nanoparticles can selectively bind into one of the blocks.[4,5]

CdS nanoparticles with surfaces modified by ethanol functional groups, M-CdS, have been synthesized for better solubility in organic solvents. Furthermore, M-CdS can selectively tether to PEO chains through hydrogen bonding and disperse well in the PEO domains of PS-*b*-PEO. Previously, we qualitatively reported the morphological transformation of the PS-*b*-PEO diblock copolymer from a hexagonally packed cylindrical structure to a body-centered cubic (bcc) or simple cubic (sc) structure[6] due to the incorporation of M-CdS nanoparticles.[7] In the present study, we focus on the evolution of dispersion of M-CdS, from DMF solutions, the PS-*b*-PEO block copolymer, to the final copolymer composite films, using small-angle X-ray scattering (SAXS) and TEM. Benefiting from the high electron density of CdS, SAXS is an advantageous tool to quantitatively study the size and aggregation of CdS-related nanoparticles, as demonstrated in the literature.[8,9]

* Corresponding author: Fax +886 3 5783813; Ph +886 3 5780281, Ext. 7108; e-mail usjeng@nsrrc.org.tw.

2. SAXS Modeling

2.1. For Colloidal Solutions. The small angle scattering (SAS) intensity distribution for colloidal particles of a monodisperse size is usually modeled as[10]

$$I(Q) = n_p P(Q) \, S(Q) \qquad (1)$$

where n_p is the number density of particles, $P(Q)$ the intraparticle structure factor (form factor), and $S(Q)$ the interparticle structure factor (structure factor). The magnitude of the wave vector transfer $Q = 4\pi \sin(\theta/2)/\lambda$ is defined by the scattering angle, θ, and the wavelength, λ, of X-rays. Considering a system of polydisperse homogeneous spheres with a dilute particle concentration, $S(Q) \sim 1$, we have

$$I(Q) = \sum_i n_p(r_i) \, P(Q,r_i) = \langle n_p \rangle \int P(Q,r) f(r) \, dr =$$
$$\langle n_p \rangle \langle P(Q) \rangle \quad (2)$$

Here, $n_p(r) = \langle n_p \rangle f(r)$ is the number density of particles of size r, with $\langle n_p \rangle$ representing the mean number density and $f(r)$ the normalized size distribution function. For the often-used Schultz distribution[11]

$$f(r) = \left(\frac{z+1}{r_a}\right)^{z+1} r^z \exp\left[-\left(\frac{z+1}{r_a}\right)r\right]\Big/\Gamma(z+1), \quad z > -1 \qquad (3)$$

where r_a is the mean radius and z is the width parameter relating to the polydispersity $p = (\langle r^2 \rangle - \langle r \rangle^2)^{1/2}/\langle r \rangle = (z+1)^{-1/2}$. The most-probable radius deduced from this distribution is $r_p = zr_a/(z+1)$. With the Schultz distribution and a volume fraction η for polydisperse spheres in a solution, we have $\langle n_p \rangle = \eta/\langle V_p \rangle$ and the averaged particle volume $\langle V_p \rangle = \langle 4/3\pi r^3 \rangle = (4/3\pi)(z+2)(z+3)r_a^3/(z+1)^2$. For the spherical form
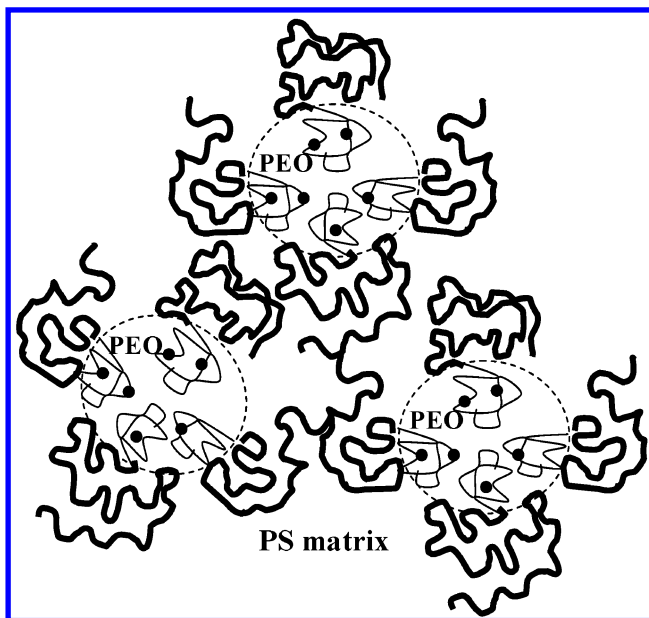
Figure 1. Cartoon of the nanoparticle/copolymer composite containing PEO domains (dotted regions) in the PS matrix. The dots inside the PEO domains represent M-CdS nanoparticles.

factor, $P(Q,r) = |F(Q,r)^2| = |\Delta\rho V_p(3j_1(Qr)/Qr)|^2$, where $\Delta\rho$ is the scattering contrast between the particles and solvent and j_1 the first-order spherical Bessel function. After the integration in eq 2, we obtain $\langle P(Q)\rangle = (\Delta\rho)^2\langle V_p^2\rangle\langle\tilde{P}(Q)\rangle = 8\pi^2(\Delta\rho)^2Q^{-6}\alpha^{z+1}G(Q)$, which leads to

$$I(Q) = \langle n_p\rangle\langle P(Q)\rangle =$$
$$\eta(4/3\pi r_a^3)(\Delta\rho)^2\frac{(z+6)(z+5)(z+4)}{(z+1)^3}\langle\tilde{P}(Q)\rangle \quad (4)$$

with $\alpha = (z+1)/Qr_a$ and $G(Q) = \alpha^{-(z+1)} - (4+\alpha^2)^{-(z+1)/2}\cos[(z+1)\tan^{-1}(2/\alpha)] + (z+2)(z+1)\{\alpha^{-(z+3)} + (4+\alpha^2)^{-(z+3)/2}\cos[(z+3)\tan^{-1}(2/\alpha)]\} - 2(z+1)(4+\alpha^2)^{-(z+2)/2}\sin[(z+2)\tan^{-1}(2/\alpha)]$.[12] Since $\langle\tilde{P}(Q)\rangle$ in eq 4 represents a normalized form factor, namely $\langle\tilde{P}(0)\rangle = 1$, the zero-$Q$ intensity $I(0)$ grows as the mean particle size grows, which serves as a good indication for particle aggregation.

2.2. For Composite Films. For nanoparticle-embedded copolymer films of a micelle-like structure (see Figure 1), we may use eq 1 for describing the corresponding SAXS profile, with n_p, $P(Q)$, and $S(Q)$ representing respectively the number density, the form factor, and the structure factor of the nanoparticle-embedded domains, in our case, PEO/M-CdS (dotted circles in Figure 1) immersed in the PS matrix of the PS-*b*-PEO copolymer.

Following the core–shell form factor,[13,14] we may express the form factor of the PEO/M-CdS domains in PS matrix as

$$P(Q) = |F_1(Q) + F_2(Q)|^2 \quad (5)$$

with $F_1(Q) = F_{CdS}(Q)\sum_{i=1}^{N}e^{i\mathbf{Q}\cdot\mathbf{r}_i}$ for N number of M-CdS nanoparticles in a PEO domain. Here, $\mathbf{r}_i$ is the distance between the centers of the PEO domain and the ith individual nanoparticle embedded in the domain, and $P_{CdS}(Q) = |F_{CdS}(Q)|^2$ is the form factor of M-CdS. For the second term in eq 5, $P_{PEO}(Q) = |F_2(Q)|^2$ is the form factor of the PEO domains (dotted circles in Figure 1).

Unfolding the square in eq 5, we have

$$P(Q) = |F_{CdS}(Q)|^2\sum_{i,j=1}^{N}e^{i\mathbf{Q}\cdot\mathbf{r}_i} +$$
$$\left|F_{CdS}(Q)\,F_2(Q)\sum_{i=1}^{N}2\cos(\mathbf{Q}\cdot\mathbf{r}_i)\right| + |F_2(Q)^2$$
$$\approx NP_{CdS}(Q)S_{CdS}(Q) + P_{PEO}(Q) \quad (6)$$

In the above, we have neglected the cross term, which approaches zero when N is large due to the cosine phase factor. Furthermore, for a small volume fraction of M-CdS in the PEO domain, the structure factor for the nanoparticles $S_{CdS}(Q) \approx 1$. Therefore, eq 6 can be simplified to $P(Q) \approx NP_{CdS}(Q) + P_{PEO}(Q)$, and the scattering for the nanoparticle–copolymer composite containing micelle-like PEO/M-CdS domains becomes

$$I(Q) \approx n_{PEO}[NP_{CdS}(Q) + P_{PEO}(Q)]S(Q)$$
$$= [n_{CdS}P_{CdS}(Q) + n_{PEO}P_{PEO}(Q)]S(Q) \quad (7)$$

For nonionic micelle-like domains, we can approximate the structure factor $S(Q)$ in eq 7 with the commonly used hard-sphere structure factor for micellar solutions.[15] The hard-sphere structure factor is characterized by two parameters: the volume fraction η and hard-sphere diameter σ. For polydisperse PEO domains, we may use the mean form factor shown previously in eq 4, with a mean structure factor $\langle S(Q)\rangle$, as detailed in ref 10. Further, we approximate $\langle S(Q)\rangle$ by an effective one-component structural factor, having the same total domain number and volume fraction of PEO as the real system.[10] In this approximation, the effective hard-sphere diameter for the polydisperse PEO domains can be determined from $\sigma^3 = 2\langle f(R,z)R^3\rangle$, where R is the radius of the PEO domains and $f(R,z)$ is the corresponding Schultz size distribution.

3. Experimental Section

Surface-modified CdS nanoparticles were synthesized by reacting cadmium acetate dehydrate (Cd(Ac)$_2$·2H$_2$O), sodium sulfide (Na$_2$S), and mercaptoethanol (HSC$_2$H$_4$OH) in methanol, using a variation of the kinetic trapping method.[16,17] After filtration, the resulting nanoparticles CdS(SC$_2$H$_4$OH)$_x$ (M-CdS) have a better solubility in *N,N*-dimethylforamide (DMF), compared to the CdS nanoparticles of bare surfaces.[6]

Isotropic and light-yellow DMF solutions, containing 0.035 wt % of M-CdS, were prepared for size characterization using UV light absorption and SAXS. Solutions of the same M-CdS concentration, but with 2.5 wt % polystyrene-*block*-poly-(ethylene oxide) (PS-*b*-PEO) copolymer added under stirring, were also prepared for SAXS as well as for film cast. The asymmetric copolymer used has a molecular weight of 125K/16.1K and a polydispersity of 1.04, with a PEO volume fraction (v/v) of 11%. The nanoparticle–copolymer mixture was dried slowly under vacuum at 323 K for a composite film, M-CdS-(1), of 1.8% M-CdS volume fraction with respect to the PEO. The resultant film of ~1 mm thickness was subsequently annealed at 383 K for 24 h for cure. Using the same procedure but with four (7.2% v/v) and 8-fold (14.4% v/v) M-CdS concentrations with respect to the PEO in the same copolymer solution of 2.5% PS-*b*-PEO, we also prepared two other composite films, M-CdS(4) and M-CdS(8), respectively.

SAXS for the composite films were measured using an 8 m SAXS instrument at the National Tsing-Hua University, Hsinchu, Taiwan,[18] with a beam wavelength of 1.54 Å monochromated from a rotating anode X-ray source at a power of 40 kV and 200 mA. Collimated by three pinholes arranged in
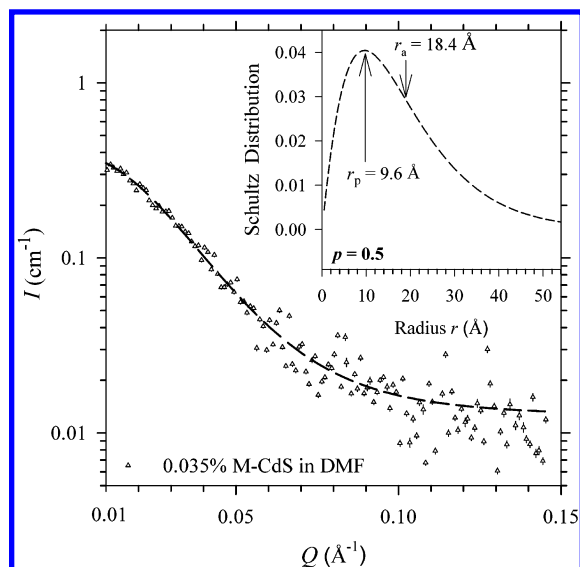
Figure 2. SAXS data for the DMF solution of 0.035 wt % M-CdS nanoparticles, fitted (dashed curve) using the Schultz size distribution with the mean radius r_a and polydispersity p values shown in the inset. The peak value r_p is the most likely observed radius in the distribution.

Figure 3. SAXS data (triangles) for a mixture of M-CdS nanoparticles (0.035 wt %) and PS-*b*-PEO (2.5 wt %), with the copolymer contribution subtracted. The data were fitted (dashed curve) using the Schultz size distribution with a mean radius 23.6 Å and a polydispersity of 0.68 for the nanoparticles. Also shown are SAXS data (diamonds) for the pure copolymer solution with the same concentration as the mixture.

three meters, the 1 mm diameter beam has a flux of $\sim 2 \times 10^6$ photons/s at the sample position. We observed circular symmetrical SAXS patterns for all the sample films from a two-dimensional area detector. For the solution samples of weak scattering and the temperature-dependent measurements of the composite films (up to 200 °C), we employed the high flux SAXS setup at the wiggler beamline BL17B of the National Synchrotron Radiation Research Center (NSRRC) of Taiwan.[19] The incident beam, monochromated to a wavelength of 1.60 Å, was collimated by two sets of slits, 0.4×0.4 mm² and 0.4×0.6 mm², resulting in a photon flux $\sim 10^9$ photons/s at the sample position. With the sample films sandwiched between two Kapton windows, the 5 cm position-sensitive linear detector, located 960 mm behind the sample position, collected the scattered photons in a Q range of 0.01−0.15 Å⁻¹. All the SAXS data were corrected for sample transmission, background, and the detector sensitivity and normalized to the absolute scattering scale $I(Q)$, namely, the differential scattering cross section dσ/dΩ per unit sample volume.[20]

4. Results and Discussion

4.1. M-CdS in DMF. Figure 2 shows the SAXS data for the M-CdS solution in DMF. The data can be simulated reasonably well (dashed curve) using a spherical shape and the Schultz size distribution shown in the inset. The two key parameters of the size distribution obtained from the fitting process are the mean radius $r_a = 18.4$ Å and the polydispersity $p = 0.5$. The most probable radius, r_p, calculated is 9.6 Å. To reduce fitting parameters, we have fitted the data in an absolute scattering intensity scale, using the M-CdS concentration 0.035 wt % and a scattering-length density (SLD) of 8.78×10^{-6} Å⁻² for DMF while 49.85×10^{-6} Å⁻² for M-CdS nanoparticles of a density of 6.63 g/cm³. The density for M-CdS is estimated from the X-ray diffraction data for the M-CdS powder. The mean radius obtained from the SAXS result is consistent with the value of 17.2 Å, as determined from the light absorption measurement.[6]

In Figure 3, we show the SAXS data for M-CdS dispersed in the PS-*b*-PEO copolymer solution, with the scattering contribution from the copolymer subtracted. Compared to the SAXS data for pure M-CdS in DMF, the noticeable increase in $I(0)$, but otherwise similar
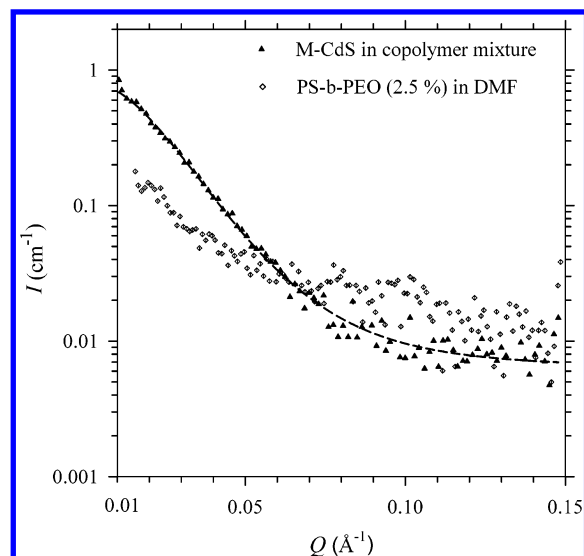
profile, reveals that M-CdS aggregates to a certain degree in the copolymer solution. Using the same polydisperse model as was used previously, we can also fit (dashed curve in Figure 3) the SAXS data for M-CdS in the copolymer solution using a larger mean radius of 23.6 Å and a polydispersity of 0.68.

The slight aggregation of M-CdS observed may be induced by the copolymers in the mixture. With the 2.5 wt % concentration in the range of semidilute concentrations,[21] PS-*b*-PEO chains spread over the solution and divide the solution space roughly into PEO domains (11% v/v) and PS domains (89% v/v). The M-CdS nanoparticles which hydrogen bond with the PEO chains, therefore, reside preferentially in the PEO blocks of smaller spacing than that in pure DMF. The higher local M-CdS concentration may facilitate the aggregation. Nevertheless, because of intervening PEO chains, the nanoparticles do not aggregate significantly either and can remain stable in the mixture for several weeks. M-CdS nanoparticles in pure DMF solutions, however, gradually form visible colloids in a few days after dispersing in DMF.

Since the solvent becomes even poorer toward the PS blocks after the nanoparticles bind to the PEO blocks—due to the hydrogen bonding between the PEO/M-CdS and DMF of a relatively high polarity—PS blocks preferentially form domains in the PEO + M-CdS + DMF environment. Dipping the complex solutions on the carbon-coated copper net for TEM imaging, we have observed spherical PS domains with diameters around 45 nm, with the M-CdS/PEO dangling on the outskirts of the PS domains. The result suggests that the formation of the micelle-like PEO−nanoparticle domains in the films (see below) occurs during the solvent drying process instead of in the solution. It is likely that in the drying process the loss of DMF solvent reverses the host−guest roles of the two phases of PS and PEO + M-CdS + DMF and finally leads to a structural inversion for forming the micelle-like domains of PEO + M-CdS in the cast films, with PS as the matrix (see the TEM images shown below).
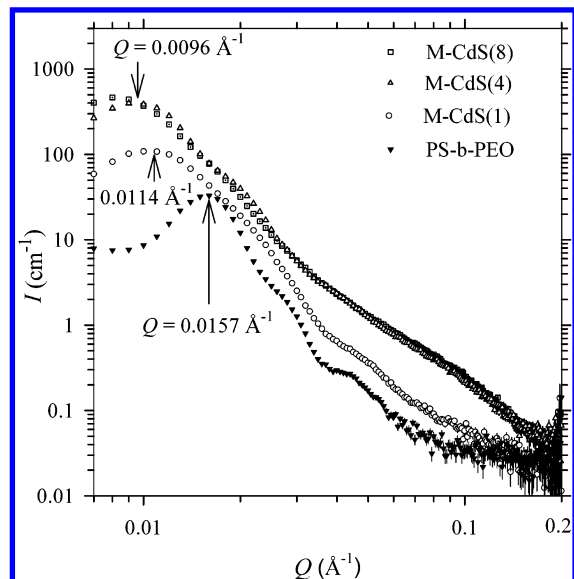
Figure 4. SAXS data for the pure copolymer film and the composite films M-CdS(1), M-CdS(4), and M-CdS(8). The arrows indicate the first scattering peak positions, corresponding roughly to the interdomain distances.

Figure 5. Comparison of SAXS profiles for the M-CdS(4) composite film measured at 30 and 200 °C. The inset shows SAXS data measured for the pure PS-*b*-PEO copolymer at 30 and 100 °C. Note that at 100 °C the profile of the pure copolymer is structureless after $Q \sim 0.06$ Å^{-1}.

4.2. M-CdS in the Composite Films. The SAXS profiles measured for the composite films (Figure 4) show quite a few prominent features. From the data in the higher-Q region ($Q > 0.06$ Å^{-1}), we found that the SAXS intensities for the composite films are considerably higher than that for the pure copolymer film. Notably, the intensity for the composite films grows nearly linearly with the M-CdS concentration for the M-CdS(1) and M-CdS(4) films. We, therefore, mainly attribute the scattering intensity in the higher-Q region to the M-CdS nanoparticles of a high SLD, equal to 49.85×10^{-6} Å^{-2} (6.63 g/cm^3), in the PEO blocks. On the other hand, the scattering contrast is low between PS and PEO blocks, having SLD values of 9.69×10^{-6} Å^{-2} (or 1.052 g/cm^3) and 10.41×10^{-6} Å^{-2} (1.124 g/cm^3), respectively.[22] Furthermore, the SAXS intensity for the M-CdS(8) film is nearly the same as that for the M-CdS(4) composite film, implying that the copolymer is saturated with M-CdS in the M-CdS(4) film, namely, 7.2% (volume fraction) nanoparticles in the PEO domains.

In the lower-Q region of Figure 4, the SAXS profiles for the films show several broad peaks of a powder-crystalline-like ordering that can be characterized by a hexagonally packed cylindrical structure for pure PS-*b*-EO and a bcc or sc structure for the composite films (detailed in our previous report).[6] We attribute this drastic morphological difference in the copolymer films to the binding of nanoparticles. For films of higher M-CdS concentrations, the first peak position shifts toward smaller Q, corresponding to a larger domain spacing of PEO/M-CdS (see Figure 1). Since all these films have the same PEO volume fraction (11%), the enlarged domain spacing implies an enlargement of the PEO domain size in the composite films for a conservation of the PEO volume. This speculation is supported by TEM images for the films, which show the tendency of increasing PEO/M-CdS domain size with the M-CdS concentration in the composite films. The result suggests that the composite system favors a structure of larger PEO domains due to a strengthened segregation power upon the embedment of M-CdS in the
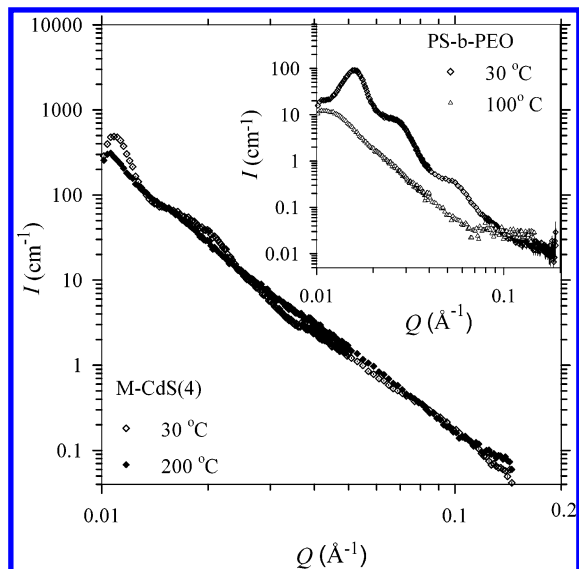
PEO blocks. This is reasonable because of the stronger interfacial interactions between PEO blocks and M-CdS nanoparticles due to hydrogen bonding. The struggle between interfacial energy (interfaces of PEO–PS, PEO–M-CdS, and PS–M-CdS), energy of crystallization (PEO), and entropy of the system, to create a minimum free energy in the composite film, may finally lead to the ordered morphology that is different from the pure copolymer.[6] Detailed analysis for the morphology transformations observed in the system, including the order–disorder transition,[7] will be discussed elsewhere on the basis of thorough temperature-dependent SAXS data and TEM images. Here, we focus on the aggregation behavior of the M-CdS in the composite films.

The extraction of the nanoparticles' structural information from the SAXS profile for the composite films is, nevertheless, hampered by the characteristic ordering peaks of the copolymer domains, which strongly modulate the scattering contribution of M-CdS (see eq 7).[23] In the following, we intend to remove or reduce the scattering contribution of the copolymer domains, by raising sample temperature, for a cleaner SAXS contribution from the nanoparticles. In Figure 5, we show the SAXS result for the M-CdS(4) composite film, measured at 200 °C—a temperature much higher than the melting and glass transition temperatures of the PEO (∼40 °C) and PS (100 °C) blocks.[6,24] At 200 °C, the scattering peaks in the lower-Q region diminish largely, indicating the disordering of the PEO/M-CdS domains in the copolymer matrix. Whereas in the higher-Q region (dominated by the nanoparticles), the SAXS profile persists surprisingly well, in both shape and intensity, revealing that the PEO/M-CdS domains are stable during the large temperature transition. Overall, the integrated scattering intensity for the composite film, $Q_{inv} = \int_0^\infty I(Q)Q^2 \, dQ$, remains nearly the same as that at room temperature, strongly suggesting that the degree of phase separation, $Q_{inv}/Q_{inv-ideal}$, between the PEO/M-CdS domains and the PS matrix, is inert to the temperature change.[25] Here $Q_{inv-ideal} = 2\pi^2\eta(1 - \eta)(\Delta\rho)^2$ is the integrated scattering intensity for an ideal two-
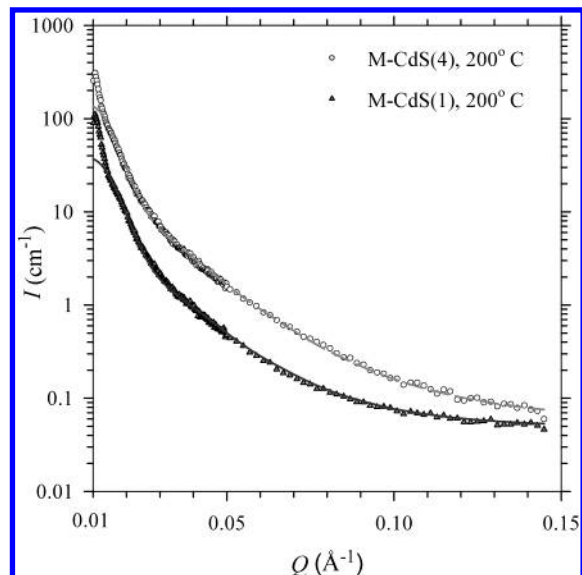
Figure 6. SAXS data for both M-CdS(4) and M-CdS(1) composite films at the molten state can be fitted (dashed and solid curves) reasonably well using eq 7. In the Q region close to 0.01 Å^{-1}, both sets of data deviate from the fitting curves and can be further characterized by $I(Q) \propto Q^{-4}$. This may indicate the existence of unknown large domains with smooth interfaces in the composite films.[24]

phase system of sharp boundary,[25,26] in our case, PEO/M-CdS domains in PS matrix. Despite the loss of the mesomorphic order at 200 °C, the SAXS result shows that PEO/M-CdS domains persist, maintaining their individual integrity without disassociating into the PS matrix. This picture is indeed visualized in the corresponding TEM image (Figure 7b) taken for the film structure frozen at 200 °C.

In contrast, the scattering invariant, Q_{inv}, for the pure copolymer film, of a PEO crystal melting temperature ~40 °C,[6] is very sensitive to temperature changes and decreases quickly to only 18% of that at room temperature (inset in Figure 5), even upon a moderate temperature increase to 100 °C ($\sim T_g$ of the PS block).[6] Using the molecular weight and the volume fraction of the PS-*b*-PEO copolymer, we can also calculate a consistent order−disorder transition temperature $T_{ODT} = 94$ °C for the pure copolymer, based on the temperature-dependent interaction parameter proposed by Zhu et al.[22] and the universal phase diagram by Leibler.[27]

Now that the ordering structure of the copolymer in the composite film dissociates at the molten state, with the PEO/M-CdS domains preserved, we can treat the molten composite as a colloidal-like system consisting of micelle-like PEO/M-CdS domains immersed in the PS matrix (Figure 1). The SAXS for the molten composite, then, is modeled by the scattering formulism outlined in eq 7, with polydisperse form factors for the PEO domains and the M-CdS nanoparticles (see eq 4). Using the Schultz size distribution and a density parameter for the PEO domains to adjust the contrasts between PEO−nanoparticles and PEO−PS simultaneously, we simulate the SAXS data for the M-CdS(4) and M-CdS-(1) films at the molten state in an absolute scattering intensity. We emphasize the merits of using the absolute scattering intensity in reducing fitting parameters and extracting the density of the individual phase of the system.

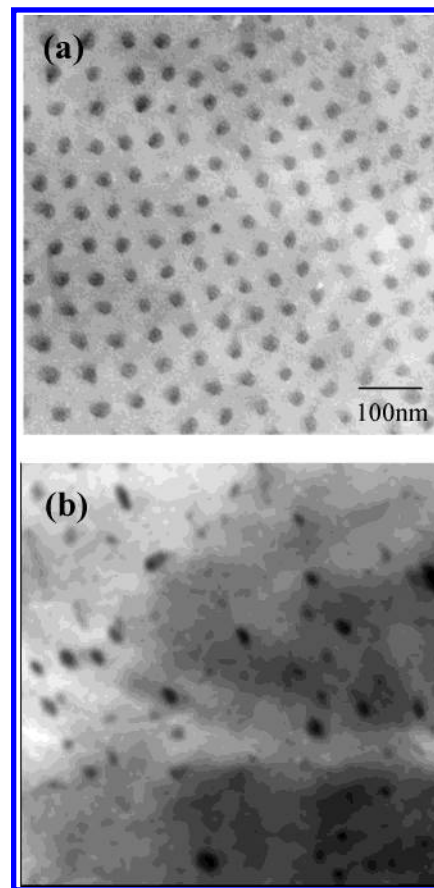The positive fitting result shown in Figure 6 strongly favors the micelle picture we proposed for the molten

Figure 7. TEM images for the M-CdS(4) composite at (a) 30 and (b) 200 °C. The dark spherical regions in (a) and (b) are the PEO/M-CdS domains. The bar in (a) represents a unit length of 100 nm for both images.

Table 1. Fitting Parameters Used for SAXS Data of M-CdS Nanoparticles in DMF Solution, M-CdS in Copolymer Solution of 2.5 wt % PS-*b*-PEO, and Copolymer Composite Films M-CdS(1) and M-CdS(4)[a]

sample status	M-CdS DMF (30 °C)	M-CdS/ PS-*b*-PEO DMF (30 °C)	M-CdS(1) film (200 °C)	M-CdS(4) film (200 °C)
r_a (Å)	18.4 ± 0.5	23.6 ± 0.2	23.2 ± 3.7	22.9 ± 3.3
p (M-CdS)	0.5 ± 0.05	0.68 ± 0.05	0.58 ± 0.04	0.49 ± 0.05
R_a (Å)			135 ± 11	140 ± 11
p (PEO)			0.26 ± 0.04	0.26 ± 0.08
d_{PEO} (g/cm^3)			0.87 ± 0.2	0.74 ± 0.1

[a] Here, p is the polydispersity for the M-CdS nanoparticles with a mean radius of r_a or for the PEO domains with a mean radius of R_a, and d_{PEO} is the density for the PEO blocks in the composite films at 200 °C.

composite. Table 1 lists all the obtained fitting parameters. In the fitting process we have fixed the densities of the M-CdS and PS phases, with the PS density $d_{PS} = 0.9639$ g/cm^3 (for 200 °C) adapted from Zhu et al.[22] As shown in Table 1, the size information for the nanoparticles in the composite films is similar to that in the solution, implying a good dispersion of the nanoparticles in the copolymer films as well.

Furthermore, the densities extracted for the PEO phase of the composite films are ~10−20% lower than the density (0.973 g/cm^3) for the PEO phase of the pure PS-*b*-PEO copolymer at 200 °C.[22] The lower density presumably results from the expansion of the PEO chains to accommodate the M-CdS nanoparticles. As a consequence, the melting or crystallization behavior of the PEO chains is significantly modified due to the

binding of the nanoparticles, as reflected in the SAXS and DSC results.[6]

From the volume fraction, η, and a mean size of $2R \sim 28$ nm fitted for the PEO/M-CdS complex domains (see Table 1), we can also estimate an interdomain distance $D \sim (4/3\pi R^3/\eta)^{-1/3} = 47$ nm. These characteristic lengths (size and spacing) revealed by SAXS for the composite films are consistent with TEM images of the composite films, which exhibit spherical-like or globular PEO/M-CdS domains of a mean diameter of ~25 nm and a mean domain spacing of ~58 nm, as illustrated in Figure 7 for the M-CdS(4) film. From the PEO domain size obtained and the volume fraction ($\sim7\%$) of the M-CdS(4) composite film, we estimate that there is an average of five M-CdS nanoparticles ($r_a = 23$ Å) in each PEO domain.

Compared to pure PEO, the much better thermal stability and the smaller PEO density (Table 1) observed for the nanoparticle-embedded PEO domains from SAXS and TEM implies that the PEO chains in the composite are more rigid and stretched due to the interactions between PEO and M-CdS. It is not surprising that the stretched and rigid chains can also suppress the crystallization of PEO blocks in the composite films at low temperature, as observed in the X-ray powder diffraction data for the composite.[6] Correspondingly, the DSC result for the composite system demonstrates an endothermal curve with little or no endothermal dip for the PEO domains containing M-CdS naroparticles.[6] All together, it is clear that the M-CdS/PEO binding inhibits individual motions of the PEO chains in the nanoparticle−copolymer composite from crystallization or melting.

5. Conclusions

From the solutions to the composite films, we have found that the surface-modified M-CdS nanoparticles can disperse well in DMF and PS-*b*-PEO copolymers with a stable size that can be described by Schultz size distributions with a mean radius of $\sim20 \pm 3$ Å and a polydispersity $\sim0.55 \pm 0.1$. We attribute the good dispersion of M-CdS to the ethanol groups (C_2H_4OH) capped on the CdS nanoparticles which hydrogen bond with DMF as well as the PEO blocks of the copolymer. The binding of the nanoparticles leads to a different morphology for the composite films with stretched PEO chains and a greatly enhanced thermal stability. Our conclusions on the nanoparticles' binding effect on the copolymer host are in concord with those given by Epps et al. in a copolymer system where segregation is promoted by a selective binding of lithium perchlorate onto the PEO blocks of the copolymer.[28]

References and Notes

(1) Park, M.; Chaikin, P. M.; Register, R. A.; Adamson, D. H. *Appl. Phys. Lett.* **2001**, *79*, 257.
(2) Urbas, A. M.; Thomas, E. L.; Kriegs, H.; Fytas, G.; Penciu, R. S.; Economou, L. N. *Phys. Rev. Lett.* **2003**, *90*, 108302.
(3) Zhang, J. Z. *Acc. Chem. Res.* **1997**, *30*, 423.
(4) Lopes, W. A.; Jaeger, H. M. *Nature (London)* **2001**, *414*, 735.
(5) (a) Bockstaller, M.; Kolb, R.; Thomas, E. L. *Adv. Mater.* **2001**, *13*, 1783. (b) Spatz, J. P.; Roescher, A.; Moller, M. *Adv. Mater.* **1996**, *8*, 337. (c) Antonietti, M.; Wenz, E.; Bronstein, L.; Seregina, M. *Adv. Mater.* **1995**, *7*, 1000.
(6) Yeh, S.-W.; Wei, K.-H.; Sun, Y.-S.; Jeng, U.; Liang, K. S. *Macromolecules* **2003**, *36*, 7903.
(7) Thompson, R. B.; Ginzburg, V. V.; Matsen, M. W.; Balazs, A. C. *Macromolecules* **2002**, *35*, 1060.
(8) Meneau, F.; Cristol, S.; Snakar, G.; Dolbnya, I.; Bras, W.; Catlow, C. R. A.; Thomas, J. M.; Greaves, G. N. *J. Appl. Crystallogr.* **2003**, *36*, 718.
(9) Dabbousi, B. O.; Rodriguez-Viejo, J.; Mikulec, F. V.; Heine, J. R.; Mattoussi, H.; Ober, R.; Jensen, K. F.; Bawendi, M. G. *J. Phys. Chem. B* **1997**, *101*, 9463.
(10) Chen, S.-H.; Lin, T.-L. In *Methods of Experimental Physics− Neutron Scattering in Condensed Matter Research*; Skold, K., Price, D. L., Eds.; Academic Press: New York, 1987; Vol. 23B, Chapter 16.
(11) Sheu, E. Y. *Phys. Rev. A* **1992**, *45*, 2428.
(12) Kotlarchyk, M.; Chen, S.-H. *J. Chem. Phys.* **1983**, *79*, 2461.
(13) Zulauf, M.; Weckstrom, K.; Hayter, J. B.; Degiorgio, V.; Corti, M. *J. Phys. Chem.* **1985**, *89*, 3411.
(14) Lin, T.-L.; Chen, S.-H.; Gabriel, N. E.; Roberts, M. F. *J. Am. Chem. Soc.* **1986**, *108*, 3499.
(15) Kinning, D. J.; Thomas, E. L. *Macromolecules* **1984**, *17*, 1712.
(16) Veinot, J. G. C.; Ginzburg, M.; Pietro, W. J. *Chem. Mater.* **1997**, *9*, 2117.
(17) Herron, N.; Wang, Y.; Eckert, H. *J. Am. Chem. Soc.* **1990**, *112*, 1322.
(18) Linliu, K.; Chen, S.-A.; Yu, T. L.; Lin, T.-L.; Lee, C.-H.; Kai, J.-J.; Chang, S.-L.; Lin, J. S. *J. Polym. Res.* **1995**, *2*, 63.
(19) Hsu, C.-H.; Lee, H.-Y.; Liang, K. S.; Jeng, U.; Windover, D.; Lu, T. M.; Jin, C. *Mater. Res. Soc. Symp. Proc.* **2002**, *612*, D5.23.1.
(20) Glinka, C. J.; Barker, J. G.; Hammouda, B.; Krueger, S.; Moyer, J. J.; Orts, W. J. *J. Appl. Crystallogr.* **1998**, *31*, 430.
(21) de Gennes, P.-G. In *Scaling Concept in Polymer Physics*; Cornell University Press: Ithaca, NY, 1980; Chapter 1.
(22) Zhu, L.; Cheng, S. Z. D.; Calhoun, B. H.; Ge, Q.; Quirk, R. P.; Thomas, E. L.; Hsiao, B. S.; Yeh, F.; Lotz, B. *Polymer* **2001**, *42*, 5829.
(23) Bendedouch, D.; Chen, S.-H.; Koehler, W. C. *J. Phys. Chem.* **1983**, *87*, 153.
(24) Zhu, L.; Chen, Y.; Zhang, A.; Calhoun, B. H.; Chun, M.; Quirk, R. P.; Cheng, S. Z. D. *Phys. Rev. B* **1999**, *60*, 10022.
(25) Chu, B.; Gao, T.; Li, Y.; Wang, J.; Desper, C. R.; Byrne, C. A. *Macromolecules* **1992**, *25*, 5724.
(26) Higgins, J. S.; Benoit, H. C. In *Polymer and Neutron Scattering*; Clarendon Press: Oxford, 1994; p 238.
(27) Leibler, L. *Macromolecules* **1980**, *13*, 1602.
(28) Epps, T. H., III; Bailey, T. S.; Pham, H. D.; Bates, F. S. *Chem. Mater.* **2002**, *14*, 1706.

MA049722R